Naval Research Laboratory

Washington, DC 20375-5000

NRL Memorandum Report 6292

A New Class of Cross Sections for Use in Atomic Scattering Calculations

G. P. MUELLER

Condensed Matter and Radiation Sciences Division

September 16, 1988

SECURITY CLASSIFICATION OF THIS PAGE

REPORT DOCUMENTATION PAGE

Form Approved
OMB No. 0704-0188

1a. REPORT SECURITY CLASSIFICATION UNCLASSIFIED	1b. RESTRICTIVE MARKINGS
2a. SECURITY CLASSIFICATION AUTHORITY	3. DISTRIBUTION / AVAILABILITY OF REPORT Approved for public release; distribution unlimited.
2b. DECLASSIFICATION / DOWNGRADING SCHEDULE	
4. PERFORMING ORGANIZATION REPORT NUMBER(S) NRL Memorandum Report 6292	5. MONITORING ORGANIZATION REPORT NUMBER(S)
6a. NAME OF PERFORMING ORGANIZATION Naval Research Laboratory 6b. OFFICE SYMBOL (If applicable) Code 4601	7a. NAME OF MONITORING ORGANIZATION
6c. ADDRESS (City, State, and ZIP Code) Washington, DC 20375-5000	7b. ADDRESS (City, State, and ZIP Code)
8a. NAME OF FUNDING / SPONSORING ORGANIZATION 8b. OFFICE SYMBOL (If applicable)	9. PROCUREMENT INSTRUMENT IDENTIFICATION NUMBER
8c. ADDRESS (City, State, and ZIP Code)	10. SOURCE OF FUNDING NUMBERS PROGRAM ELEMENT NO. / PROJECT NO. / TASK NO / WORK UNIT ACCESSION NO DN157-034

11. TITLE (Include Security Classification)
A New Class of Cross Sections for Use in Atomic Scattering Calculations

12. PERSONAL AUTHOR(S)
Mueller, G.P.

13a. TYPE OF REPORT	13b. TIME COVERED	14. DATE OF REPORT (Year, Month, Day)	15. PAGE COUNT
Interim	FROM _____ TO _____	1988 September 16	37

16. SUPPLEMENTARY NOTATION

17. COSATI CODES			18. SUBJECT TERMS (Continue on reverse if necessary and identify by block number)
FIELD	GROUP	SUB-GROUP	Cross section, Lindhard Potentials,

19. ABSTRACT (Continue on reverse if necessary and identify by block number)

It is useful to have simple cross sections to represent the interactions between particles when performing transport theory calculations for range, energy deposition, and damage by impinging ions on bulk materials. In this report I present a number of families of finite range interactions that are simple to generate during such transport calculations. These cross sections have a Thomas-Fermi character at large energy transfers and a wide variation of behavior for small energy transfers. The potentials that correspond to these cross sections are displayed graphically, so that if one has a phenomenologically derived potential between two constituents, one can read off of the graphs which family member will give a good representation of that interaction.

20. DISTRIBUTION / AVAILABILITY OF ABSTRACT	21. ABSTRACT SECURITY CLASSIFICATION
☒ UNCLASSIFIED/UNLIMITED ☐ SAME AS RPT ☐ DTIC USERS	UNCLASSIFIED
22a. NAME OF RESPONSIBLE INDIVIDUAL G.P. Mueller	22b. TELEPHONE (Include Area Code) (202) 767-6977 22c. OFFICE SYMBOL Code 4601

DD Form 1473, JUN 86 *Previous editions are obsolete* SECURITY CLASSIFICATION OF THIS PAGE

S/N 0102-LF-014-6603

CONTENTS

A NEW CLASS OF CROSS SECTIONS FOR USE IN ATOMIC SCATTERING CALCULATIONS

INTRODUCTION

In the process of calculating the range, energy deposition and damage characteristics of heavy ions in bulk materials, one needs some representation of the interactions between the impinging ions and the target constituents. Because the target atoms are displaced and themselves traverse the target, one needs the interactions between the various constituents. There is available a wide range of such potentials, from the universal ones of the Thomas-Fermi type to ones specifically tailored to reproduce the crystalline properties of particular species.

These interactions are used in three general types of radiation damage calculations. The most exacting are the molecular dynamics codes,[1,2] which simulate a small portion of a crystal in the computer. The response of the crystal to an initial displacement, caused by an incident neutron or heavy ion, is followed by simultaneously solving the equations of motion of all of the atoms in the sample crystal. More flexible, if less thorough, are such simulation codes as those of Robinson and Torrens[3] and Beeler and Besco.[4] In these the crystalline structure of the material is present in some fashion, but the moving ions are followed one at a time. The molecular dynamics codes require potentials that reproduce the major properties of the crystal. The second type of simulation code is somewhat less stringent, in part because the potentials are not allowed to act for impact parameters greater than 50-80% of the nearest neighbor distance.

Finally, there are the transport theory calculations,[5,6,7,8,9,10] which assume an amorphous material--no crystal structure is present. These calculations do not use the potentials directly, but use the associated differential cross sections. For the most part, they make use of the of the Lindhard, Nielsen and Scharff (LNS)[5] universal cross section based on the Thomas-Fermi interaction. There are a number of problems associated with this

Manuscript approved June 29, 1988.

interaction. It is known[11] be too strong for large separations. While its universal character makes it convenient to use, it does not accurately reflect the properties of more realistic potentials, especially at large separations. Phenomenological potentials are usually made to vanish for sufficiently large distances (2nd or 3rd nearest neighbor distances), whereas the Thomas-Fermi potential is of infinite range. The corresponding Thomas-Fermi cross section blows up for small energy transfers and the total cross section is infinite, unless a cutoff in energy transfer is imposed.

Our goal in this work is to create new differential cross sections (more specifically, families of them) that both more accurately reflect the properties of realistic potentials and are as easy to use as is the LNS cross section. In the next two sections we describe the Thomas-Fermi potential and its relation to various phenomenological interactions and outline the method that LNS use to obtain their cross section. We then present a new class of cross sections that reproduce the LNS form for large energy transfers (corresponding to small separations of the interacting ions), but which have flexible characteristics for small energy transfers.

Within the spirit of the approximations used by LNS, there is a method, outlined in Appendix B, that allows the potential corresponding to a given differential cross section to be easily calculated. We present a series of figures of the potentials that are generated from our new families of cross sections. By comparing a given phenomenological potential with the families thus generated, one can automatically obtain a differential cross section closely corresponding to that phenomenological potential. Finally, we give a number of examples and discuss the possible use of these new cross sections.

INTERATOMIC POTENTIALS

Before considering atomic scattering cross sections, let us look at some of the interatomic potentials on which the cross sections are based. Suppose we have an atom with atomic number Z_1 and atomic mass A_1 interacting with another atom with atomic number Z_2 and mass A_2. Firsov[12] represented the interaction between two such atoms, separated by a distance r, as a screened Coulomb potential of the form

$$V_F(r) = \frac{Z_1 Z_2 e^2}{r} \; C_T(r/a) \qquad (1$$

The quantity $C_T(r)$ is the Thomas-Fermi screening factor, which is available in tabular form.[13] The screening radius a is given by

$$a = \left[\frac{9\pi^2}{128}\right]^{1/3} \left[\frac{h^2}{4\pi^2 m e^2}\right] Z^{-1/3} = 0.88534\, a_o\, Z^{-1/3} \qquad (2$$

$$Z_F = (Z_1^{1/2} + Z_2^{1/2})^2$$

$$(3$$

$$Z_L = (Z_1^{2/3} + Z_2^{2/3})^{3/2}$$

where in expression (3) we present both the Firsov version for Z and that due to LNS. This Firsov or Thomas-Fermi (as it is more commonly called) potential is universal, in that it can represent the interactions between any pair of atoms, given only their atomic numbers and the separation between them. Because of its simplicity, this potential is widely used in atomic scattering problems.

While the Thomas-Fermi potential is on reasonably secure theoretical ground when the interatomic separations are small, it is inadequate for large separations. The Thomas-Fermi screening factor $C_T(x)$ falls off as x^{-3} for large x. On both experimental and theoretical grounds an exponential falloff is more realistic. For this reason, another universal potential, the Molière,[14,15] is also widely used. The Molière potential also has the form (1), and its screening factor reproduces the Thomas-Fermi screening factor out to reduced separations of $x \approx 6$. After that, it falls off exponentially. The Firsov, LNS, or some other suitable screening radius may be used with the Molière potential.

The best interaction to use, of course, is one that is tailored, phenomenologically, to the two interacting atoms in the solid. There are many ways of obtaining such potentials, but a commonly used one is some version of the following (for the moment, we assume $Z_1=Z_2$): For small separations, the Thomas-Fermi interaction is used. For large separations a form is used whose parameters are adjusted to reproduce some of the properties of a crystal made up of these atoms. Finally, these two portions are joined smoothly in the intermediate region. In Fig. 1 we show such an interaction, due to Erginsoy,

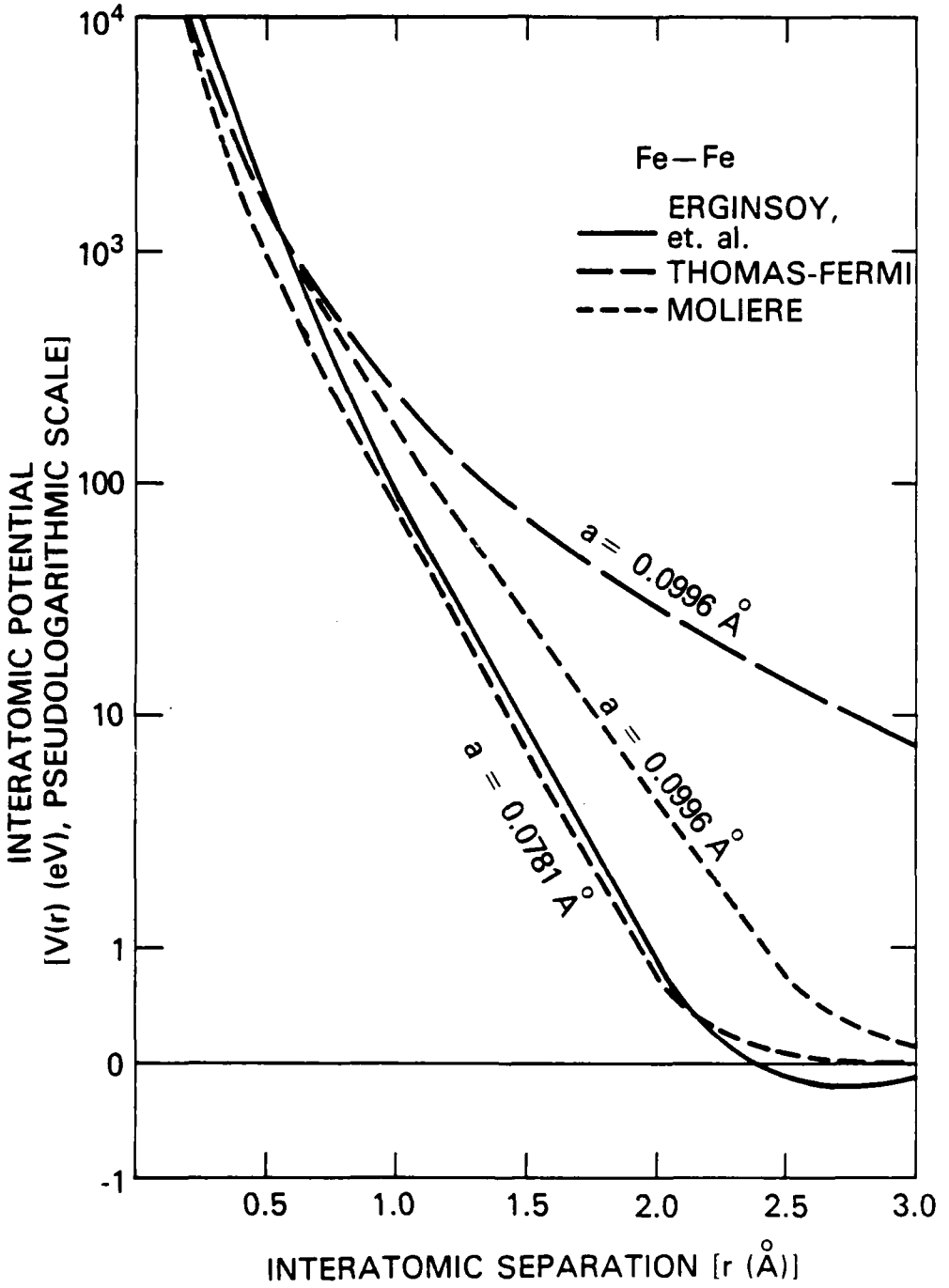

Fig. 1 — Iron-iron interatomic potentials. Shown are the Thomas-Fermi and the Molière using the Firsov screening length (0.0996 Å), the Molière with the Torrens-Robinson screening length (0.0781 Å), and the phenomenological potential of Erginsoy, et al.

Vineyard and Englert,[2] for alpha (bcc) iron. We note that this potential passes through zero at a separation somewhat less than the nearest neighbor distance (2.48 Å). This behavior is typical; it is the attractive portion of the potential in the nearest neighbor region that binds the crystal. More sophisticated potentials will oscillate about zero out to 2nd and 3rd nearest neighbor distances; the magnitude of these oscillations is of the order of 1 eV.

For comparison, we also show the Thomas-Fermi and Molière potentials for iron, using the Firsov value (0.0966 Å) of the screening radius. We see that the agreement is not bad for small separations, as we would expect, but becomes increasingly worse as the separation increases, especially for the Thomas-Fermi interaction. This again is typical; the Thomas-Fermi is too large for large separations. Finally, we show the Molière potential with the Torrens and Robinson[16] value (0.0781 Å) of the screening length. Here the agreement is quite good for large separations. Of course varying the screening length may distort the agreement at small separations.

For the purposes of transport theory calculations, the details of the potential in the region near and past the point at which it first passes through zero are of no consequence. No significant amount of energy is transferred to lattice atoms when the impact parameter lies in or beyond this region. Further, the differential cross section for an infinite range potential blows up as the energy transfer vanishes, which imposes an unnecessary complication on integral equation calculations. Rather than using a cross section based on the infinite range, Thomas-Fermi potential, these calculations would be both simpler and more realistic if we started with a finite range potential.

REVIEW OF THE LNS METHOD

In computer simulation calculations one uses the relevant potential directly to represent the interaction between atoms. In integral equation calculations, one used the differential cross section derived from that potential. Suppose that one particle with energy E and impact parameter p is moving toward another (stationary) particle. The center of mass energy is

$$E_r = A_2 \, E \, / \, (A_1 + A_2). \qquad (4$$

The scattering angle is given by[17]

$$\theta = \pi - 2p \int_{r_{min}}^{\infty} \frac{dr}{r} \left[r^2 \left[1 - \frac{Z_1 Z_2 e^2}{r E_r} C(r/a) \right] - p^2 \right]^{-1/2} \quad (5$$

where r_{min} is the largest root of the radical in the integrand. The energy transferred in the collision is

$$T = T_m \sin^2 \theta/2 \quad (6$$

$$T_m = \tau E = [4 A_1 A_2 (A_1+A_2)^{-2}] \quad E , \quad (7$$

where T_m is the maximum kinematically allowed energy transfer. Corresponding to this maximum energy transfer is the minimum energy that can be carried away by the incident particle, which is given by

$$E_{min} = E/\beta = E (A_1-A_2)^2/(A_1+A_2)^2 . \quad (8$$

Much of the work of Lindhard and his coworkers is couched in terms of the dimensionless variables

$$\epsilon = E / E_L = E [Z_1 Z_2 e^2 (A_1+A_2) / (a A_2)]^{-1} \quad (9$$

$$t = \epsilon^2 T/T_m = \epsilon^2 \sin^2 \theta/2 . \quad (10$$

In terms of these definitions the differential cross section is given by

$$d\sigma = 2 \pi p \, dp ; \quad (11$$

LNS use the notation

$$d\sigma = -(\pi a^2 /2) t^{-3/2} f(t^{\frac{1}{2}}) \, dt , \quad (12$$

so that

$$f(t^{\frac{1}{2}}) = (-4/a^2)\ t^{3/2}\ p(t)\ dp(t)/dt\ . \qquad (13$$

For lack of any standard name, we will call $f(\phi)$ the kernel of the cross section.

Out of a desire to create a simple, universal cross section, LNS make two approximations[18] to obtain $f(t^{\frac{1}{2}})$ for the Thomas-Fermi potential: they replace Eq. (5) by the momentum approximation[19] to the scattering angle, so that

$$\theta = -\frac{p}{E_r} \int_p^\infty dr\ [\ r^2 - p^2\ ]^{-1/2}\ \ \frac{d}{dr}\ V(r) \qquad (14$$

and they use the expression

$$t = 1/4\ \epsilon^2\ \theta^2 \qquad (15$$

to replace θ by t, instead of the exact expression (10). By combining these approximations we find that we can write

$$t^{1/2} = -\frac{p}{2a} \int_{p/a}^\infty dx\ [\ x^2 - (p/a)^2\ ]^{-1/2}\ \ \frac{d}{dx}\ [\ x^{-1}\ C(x)\ ] \qquad (16$$

Eq. (16) provides a functional relationship between the impact parameter and the reduced energy transfer that can be used to solve Eqs. (11-12) for $f(t^{\frac{1}{2}})$. The advantage of the LNS approximations is that the kernel of the differential cross section depends only on one variable; Eq. (16) is a relationship between t and p/a, not t, p/a and ϵ.

Given these considerations, the total (macroscopic) cross section can be written

$$N\ \sigma(E) = N\pi a^2 \int_0^\epsilon d\phi\ \phi^{-2}\ f(\phi) \qquad (17$$

where N is the number density of lattice atoms and

$$\phi = t^{\frac{1}{2}} . \qquad (18$$

Following LNS, we can write

$$N\,S(E) = N\pi a^2 \frac{\tau E_L}{\epsilon} \int_0^{\epsilon} d\phi\, f(\phi) \qquad (19$$

for the stopping power for elastic collisions and

$$N\,W(E) = N\pi a^2 \left[\frac{\tau E_L}{\epsilon}\right]^2 \int_0^{\epsilon} d\phi\, \phi^2\, f(\phi) \qquad (20$$

for the square fluctuation in energy loss.

The LNS method we just outlined could be used for other potentials, as well as the Thomas-Fermi. We will use a subscript L to refer specifically to the LNS results for the Thomas-Fermi interaction. The quantities f_L, S_L and W_L are provided by LNS in tabular form. A convenient fit to f_L, in the form

$$f_W(\phi) = k\,\phi^{1/3}\,[1 + (2k)^{2/3}\,\phi^{8/9}\,]^{-3/2}\ ,\ k=1.309 \qquad (21$$

has been created by Winterbon, Sigmund and Sanders (WSS).[8] With this form, relatively convenient expressions can be found[20,21] for σ_W, S_W and W_W; in some cases they are easier to use than the tabular forms of LNS.

NEW CROSS SECTIONS

In our discussions of interatomic potentials, we implied that it would be useful to have a potential that: (a) vanishes at a separation near the nearest neighbor distance, which distance depends on the particular material; (b), reproduces the Thomas-Fermi potential for small separations; (c), has for its corresponding differential cross section a simple, easy-to-evaluate form; (d), has simple forms for the related quantities $N\sigma(E)$, $NS(E)$ and $NW(E)$; and (e), is flexible enough to roughly match any of the phenomenologically determined interatomic potentials.

We could, of course, simply create a flexible potential form that possessed properties (a), (b) and (e), but there is no guarantee that it would possess properties (c) and (d). When using integral equation methods for calculating range and damage characteristics of heavy ions, it is the cross section, and not the potential, that is used. So instead of choosing a flexible potential form, we will choose a flexible cross section form that possesses properties (c) and (d). Property (b) is satisfied by requiring that our new cross sections look like the LNS cross section for large values of t. Because we can calculate what the potential is that corresponds to a given cross section, we can build sufficient flexibility into our new cross sections in order to satisfy (e). Finally, because we want the total cross sections to be finite, we will require that the kernel $f(\phi)$ of our cross section fall off at least as fast as ϕ^{δ}, $\delta>1$, as ϕ goes to 0; the corresponding potentials will be of finite range.

We express out new differential cross sections in the form

$$d\sigma = -\pi a^2 \phi^{-2} g(\phi)\, d\phi , \qquad (22$$

where $g(\phi)$ has the form

$$g(\phi) = \begin{cases} g_{n,m}(\phi), & \phi<\phi^* \\ g_u(\phi), & \phi>\phi^* \end{cases} \qquad (23$$

We will choose a form for $g_u(\phi)$ that reproduces the Thomas-Fermi cross section, within the approximations of the Lindhard method. For $g_{n,m}(\phi)$ we will use a number of adjustable forms. At this point, the transition value ϕ^* is another free parameter. We take

$$g_u(\phi) = (b+\phi/2)/(c+\phi(d+\phi)), \quad b=0.0074,\ c=0.0376,\ d=0.83. \qquad (24$$

In Fig. 2 we show a comparison of this $g_u(\phi)$ with the LNS $f_L(\phi)$; the values of $f_L(\phi)$ are taken from the more complete tables of Manning,[22] rather than from LNS. We see that the agreement is quite good for $\phi>0.006$. In Fig. 3 we show the percentage error in $g_u(\phi)$ and the Winterbon, Sigmund and Sanders (WSS) fit (Eq. (21)) to the LNS $f(\phi)$. On the whole, $g_u(\phi)$ fits $f_L(\phi)$ as well as does $f_W(\phi)$ over the range $\phi>0.006$. Differences of 4-6% are of no consequence

because interatomic potentials are not that well known. In addition, the LNS approximations, with respect to the exact results, introduce errors of more than 4-6%.

For $g_{n,m}(\phi)$ we use the form

$$g_{n,m}(\phi) = g_{n,m}(\phi;\phi^*) = A\,\phi^{rm/4}\,[\,B + \phi^{m/4}\,]^{-n}\,. \qquad (25$$

The values of A and B are fixed by the requirement that the values and derivatives of $g_{n,m}$ and g_u are equal at $\phi=\phi^*$. Specifically, we have

$$B = \phi^{*m/4}\,g'(\phi^*)\,[(rm/4\phi^*)\,g_u(\phi^*) - g'(\phi^*)]^{-1}\,, \qquad (26$$

$$A = \phi^{*-rm/4}\,(\,B + \phi^{*m/4}\,)^n\,g_u(\phi^*)\,, \qquad (27$$

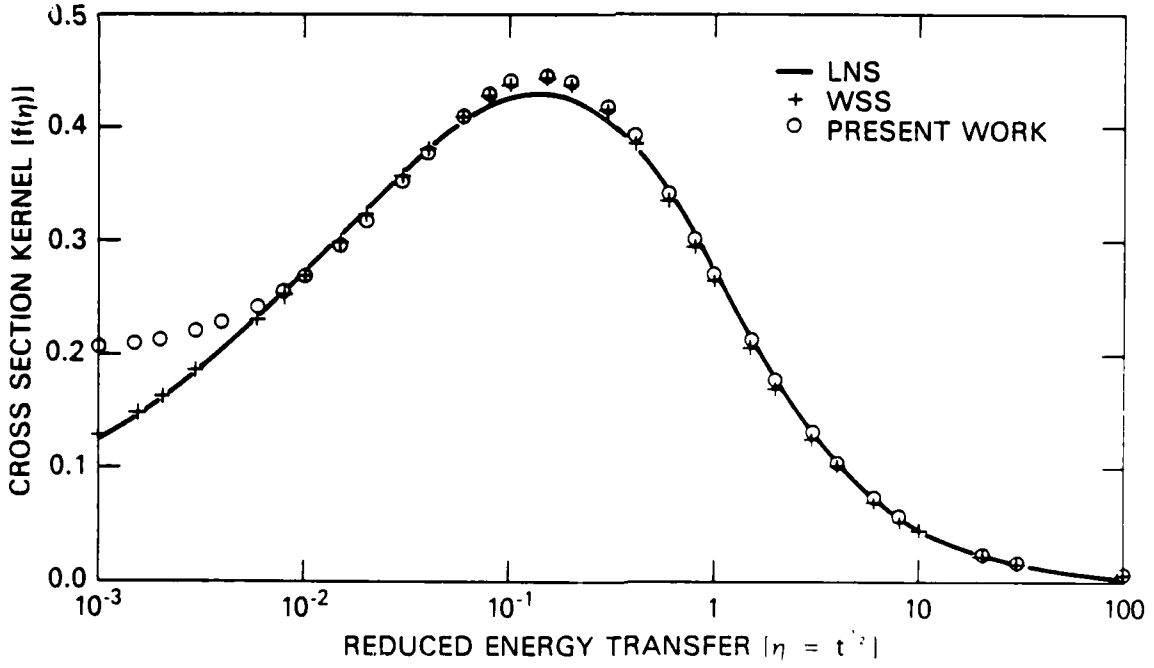

Fig. 2 — The kernel of the differential cross sections of LNS, WSS, and the present work.

where g' is the derivative of g_u. We are left with n, m and ϕ^* as parameters. We will label our families of cross sections with the notation (n,m), and will label the family members by (n,m,ϕ^*). Only a few pairs of (n,m) values, with ϕ^* adjustable, are necessary in order to give our cross section sufficient flexibility. In particular, we will make use of (n,m) = (3,2), (2,3) and (4,4).

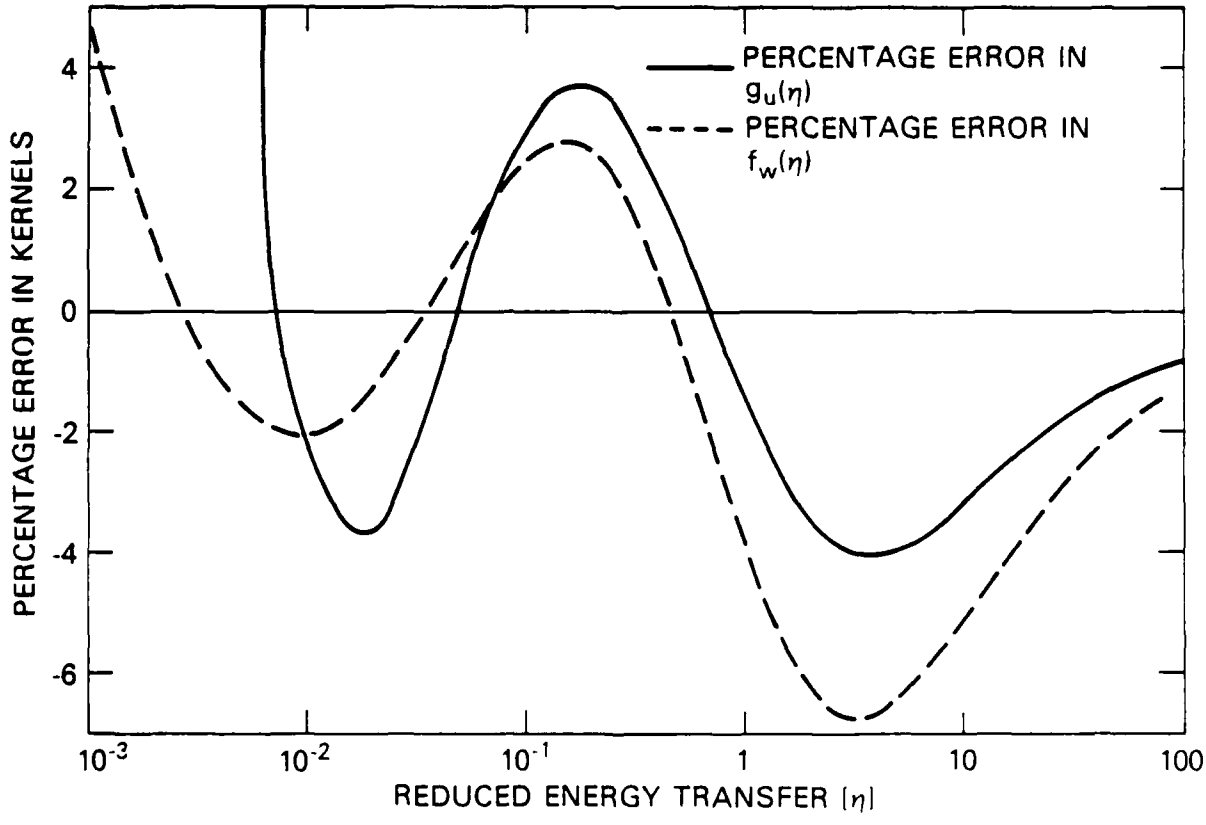

Fig. 3 — Percentage errors in the kernels of WSS and the present work, relative to the Thomas-Fermi results of LNS.

In Fig. 4 we plot, for $10^{-5}<\phi<10^{-1}$, a variety of the kernels $f(\phi)$, including $f_L(\phi)$, $f_W(\phi)$, the kernel corresponding to the Molière potential,[23] and a representative sample of the kernels from the present work. (LNS warn that their cross section is inaccurate for $\phi<10^{-3}$-10^{-2}, but their warning is seldom heeded.) We note that the differential cross section includes the factor ϕ^{-2}, so that the Lindhard and Molière total cross sections blow up as ϕ goes to zero; whereas our new total cross sections remain finite. The total cross sections and related quantities associated with the new differential cross sections are easy to evaluate; the expressions are given in Appendix A.

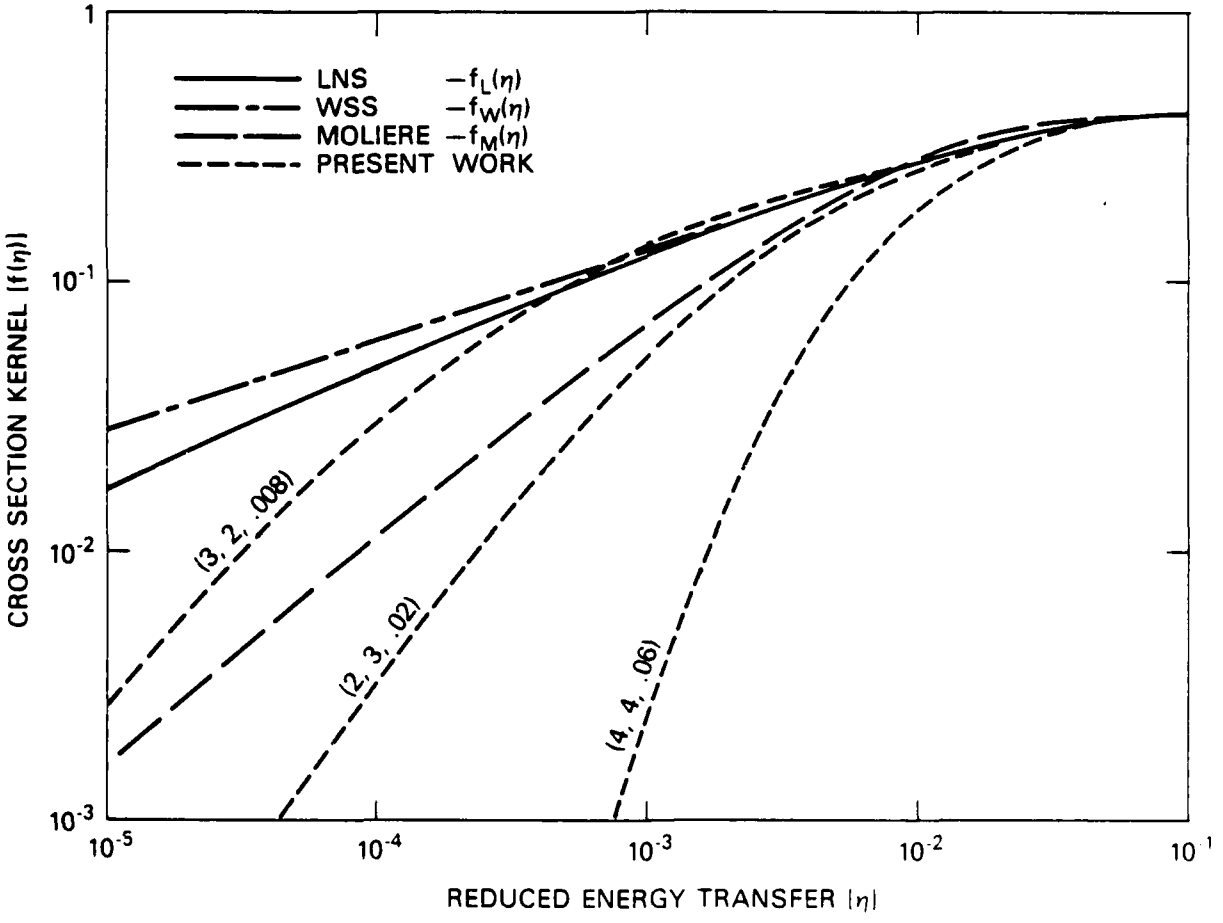

Fig. 4 — A variety of cross section kernels, plotted for low values of $t^{\frac{1}{3}}$.

FITTING PROCEDURE AND EXAMPLES

In Appendix B we outline a procedure for obtaining the potential or screening function corresponding to a given differential cross section, within the spirit of the LNS approximations. By using this procedure, we plot, in Figs. 5-7, the screening functions associated with our three families of cross sections. For a given (n,m) pair (see Eq. (25)), we show a family of screening factors with each member labeled by the value of ϕ^*.

Given a phenomenological potential, our procedure for obtaining a differential cross section is as follows: Plot the screening factor for the phenomenological potential, using the Firsov choice of screening radius,

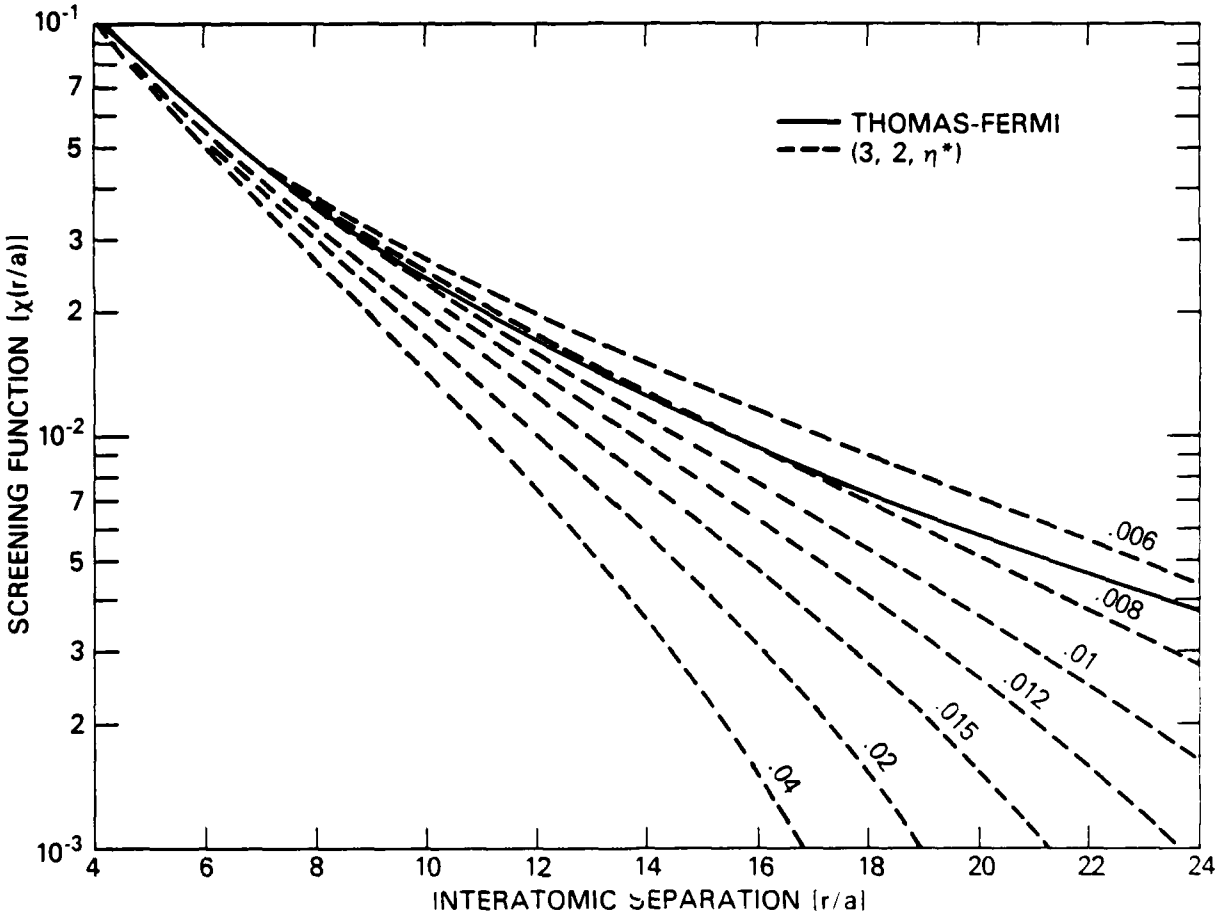

Fig. 5 — The screening functions corresponding to the (3,2) family of cross sections.

unless some specific screening radius is associated with the potential. Compare this plot with Figs. 5-7 to obtain the family member that best matches the given screening factor, recalling in the process that the fit need not be good beyond distances at which the potential is too weak (1-10 eV) to affect radiation damage and range calculations. Having obtained a fit to the screening factor with parameters (n,m, ϕ^*), Eq. (23-27) automatically yield the corresponding cross section.

As an example, we consider the Genthon potential for copper.[24] This potential is of Thomas-Fermi form out to 0.51 Å, with the Lindhard screening radius, and of Born-Mayer (exponential) form beyond that. Genthon set the

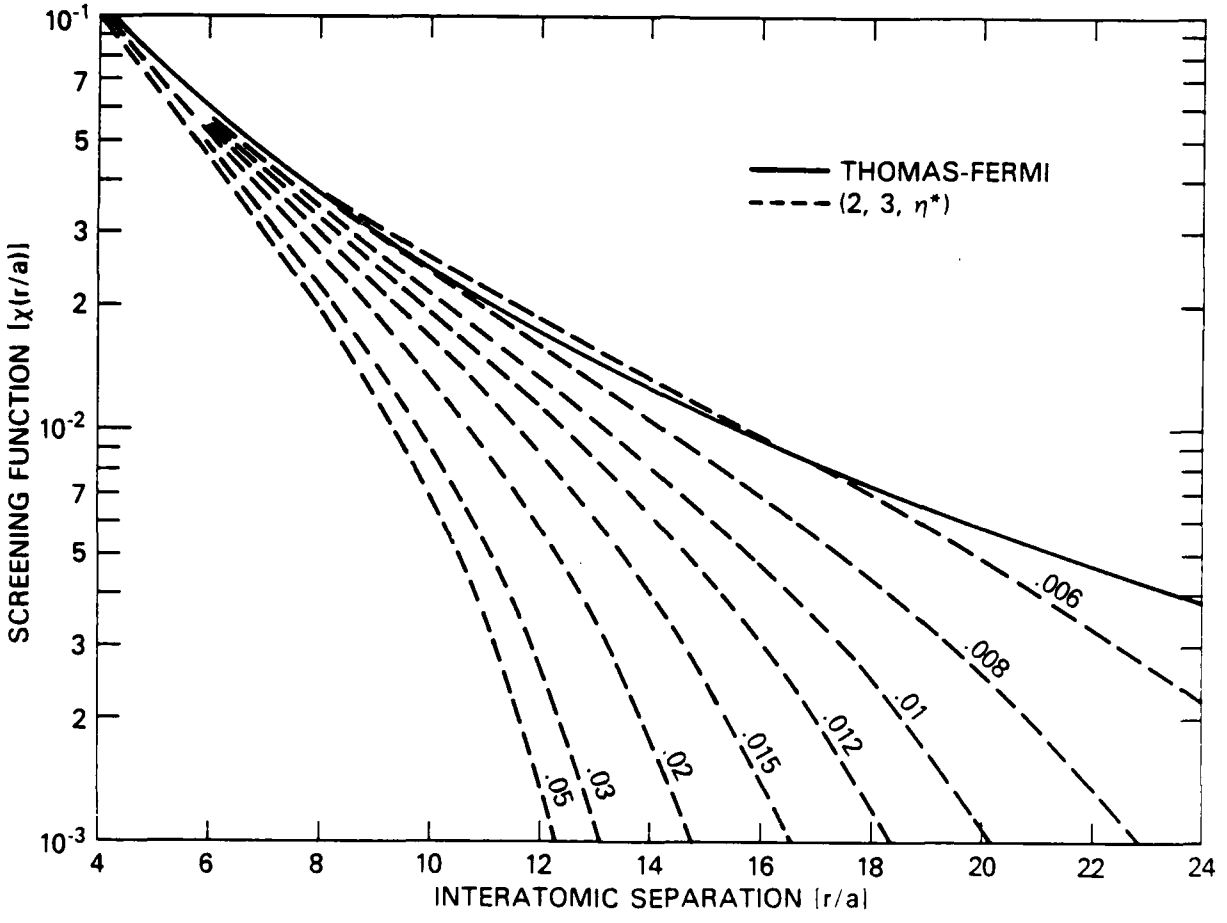

Fig. 6 — The screening functions corresponding to the (2,3) family of cross sections.

exponential decay constant so that the potential reproduced the bulk modulus for copper.[24,25] In Fig. 8 we compare the Genthon screening factor with several members of the (2,3) family; we choose (2,3, .02) to represent the corresponding Genthon cross section.

For the purpose of obtaining a Cu-Cu cross section for radiation damage calculations, we are done. But in order to examine the relations between the

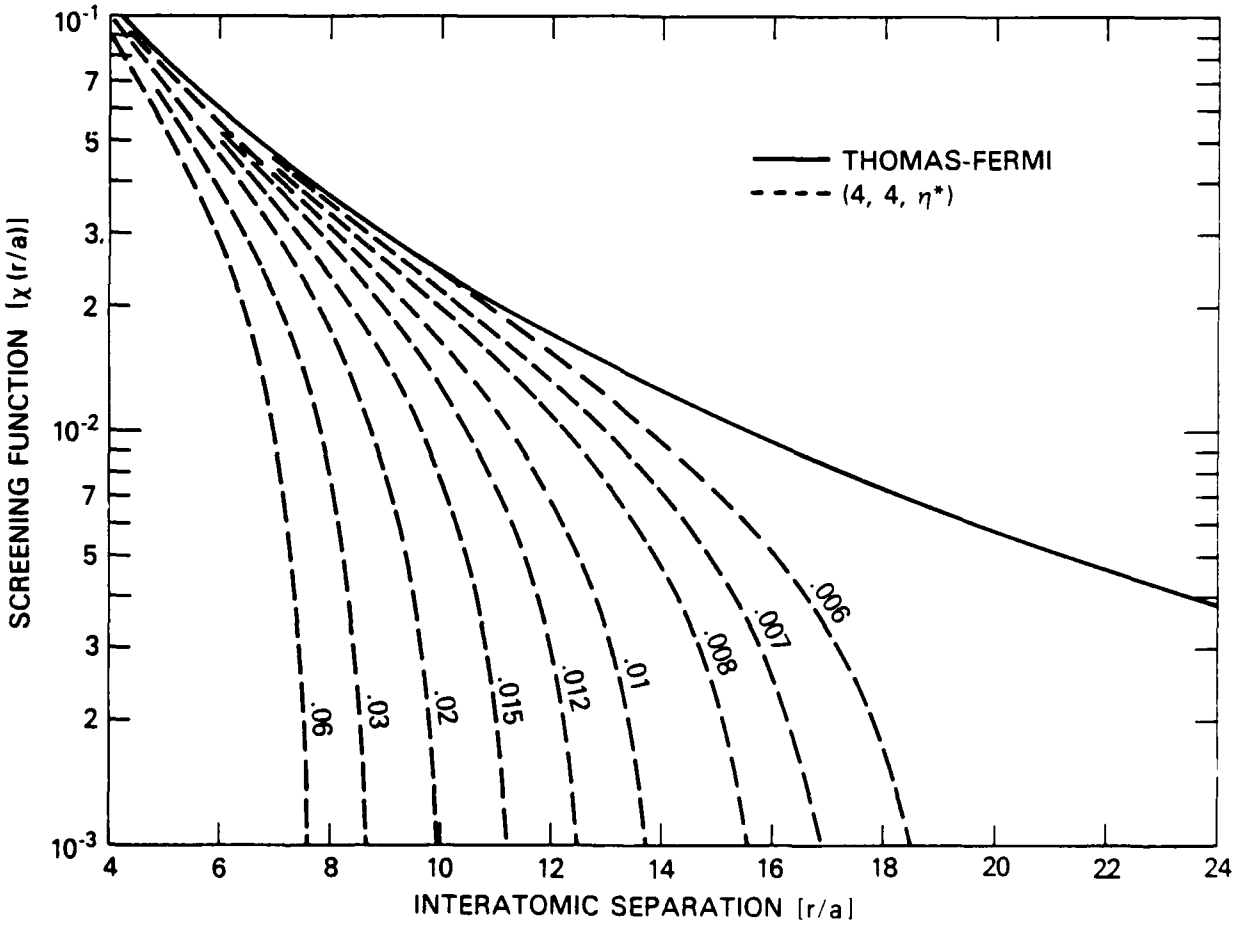

Fig. 7 — The screening functions corresponding to the (4,4) family of cross sections.

various potentials and their cross sections, we plot, in Fig. 9, the Genthon Cu-Cu potential, the potential associated with our (2,3, .02) cross section, two forms of the Molière potential, and the Thomas-Fermi potential. The Molière interaction in pictured both with the LNS screening radius (0.1078 Å) that Genthon used, and with the Torrens and Robinson Value (0.0738 Å).[16] (Torrens and Robinson chose the value of the screening radius for which the Molière potential has the same magnitude at the nearest neighbor distance as does a Born-Mayer potential whose parameters were determined from elastic constant data).

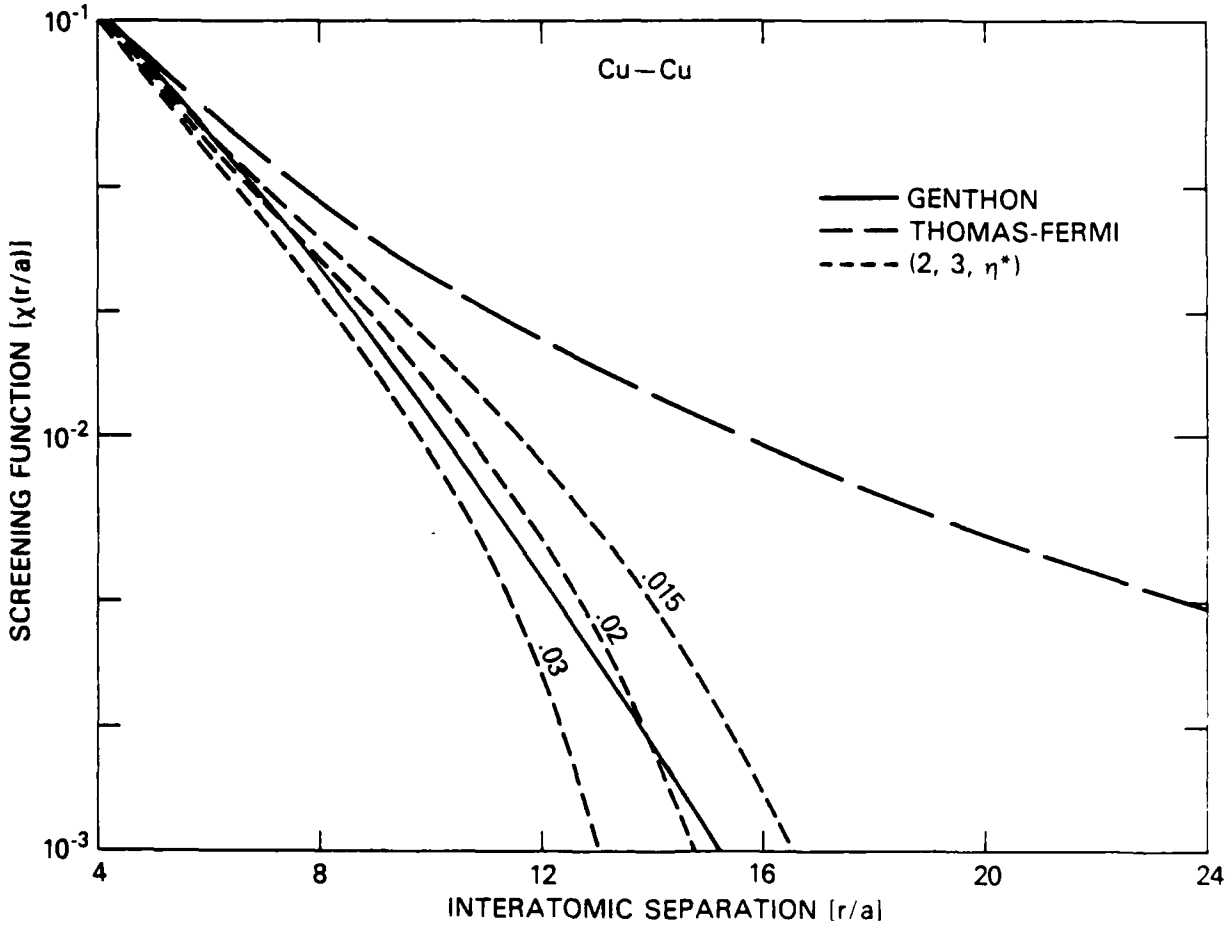

Fig. 8 — Comparison of the Genthon Cu-Cu screening function with the screening functions corresponding to several members of the (2,3) family.

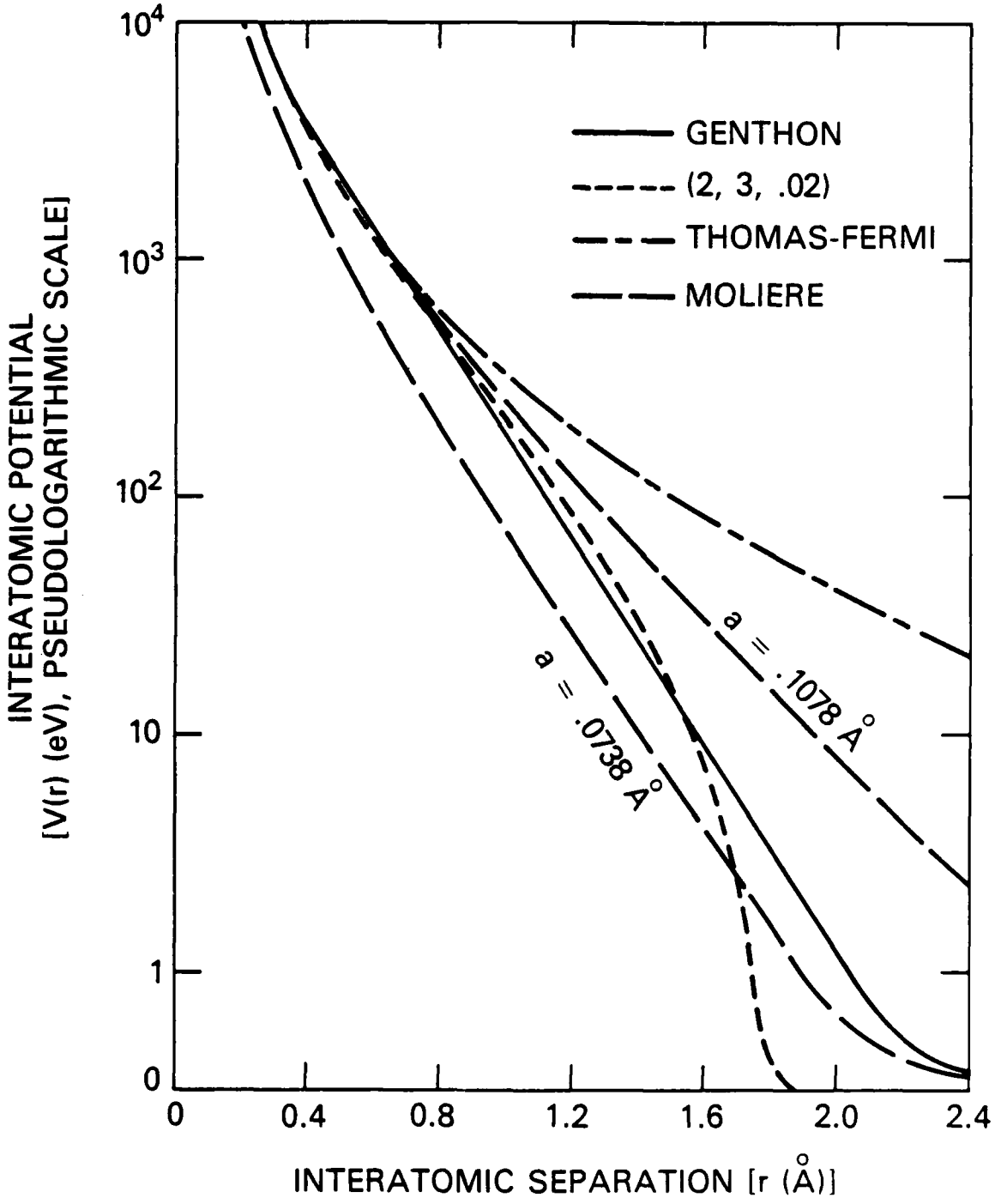

Fig. 9 — Comparison of the Genthon Cu-Cu potential with the Thomas-Fermi, the (2,3, .02), and the Molière potentials. The Molière potential is shown using both the LNS screening length (0.1078 Å) and the Torrens and Robinson screening length (0.0738 Å).

In Fig. 10 we show the stopping power NS(E) (see Eqs. (A2, A5, A13, A15)) for copper in copper based on each of the potentials shown in the previous figure. The values for the Genthon potential were obtained by the same procedure[23,19] as used by Mueller to obtain the Molière results. We see that the properties of the cross sections reflect the properties of the interactions. For higher energies, all of the cross sections give the same results with the exception of the Molière with the Torrens and Robinson screening radius, which is considerably lower. For lower energies the Torrens-Robinson-Molière and Genthon results agree, because both potentials

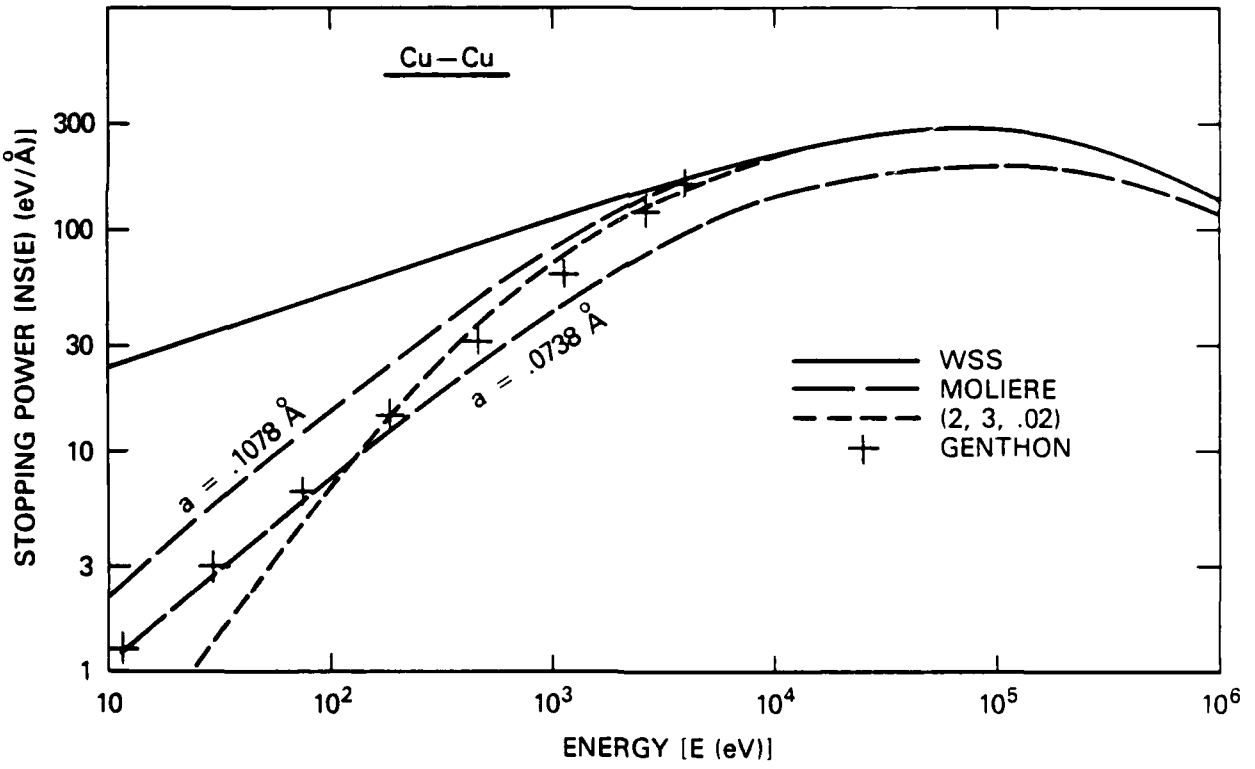

Fig. 10 — Comparison of the calculated stopping powers for copper in copper. Shown are the results based on the Genthon Cu-Cu potential, the WSS and (2,3, .02) cross sections, and the Molière potential using both the LNS screening length (0.1078 Å) the Torrens and Robinson screening length (0.0738 Å).

were fit to (low energy) crystalline properties of copper. The Thomas-Fermi results are much too large at low energies. Our cross section, the (2,3, .02), gives an adequate approximation to the Genthon over the whole range of energies. The results of using the Molière cross section with the Genthon (LNS) screening length are only fair.

As further examples, in Fig. 11 we present the screening factors, and our fits, for a number of interatomic potentials: the uranium-uranium potential of Genthon;[24] the helium-tantalum potential of Wilson and Johnson;[26] and the

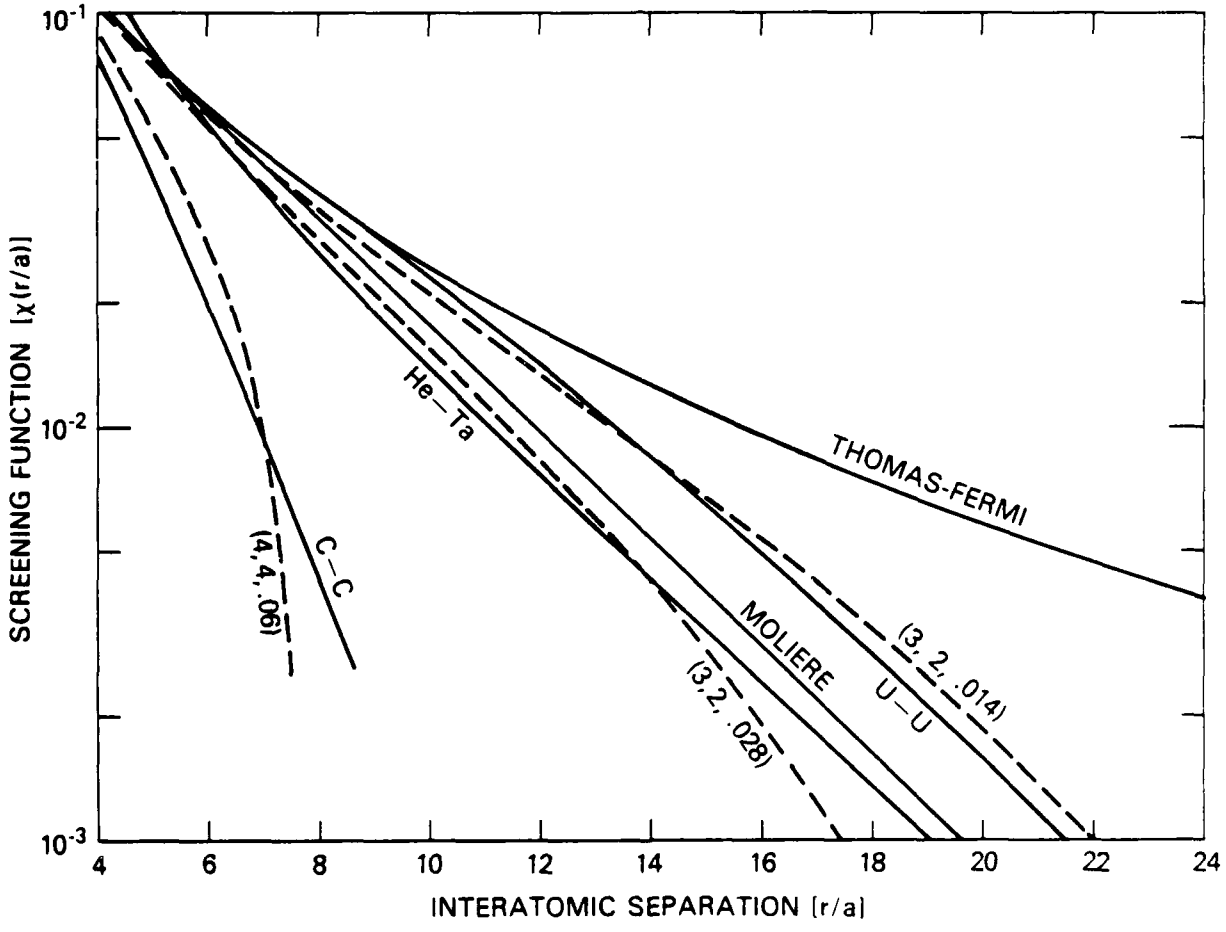

Fig. 11 — The screening functions for a variety of interatomic potentials (C-C, He-Ta, U-U), along with fits to them. Also shown are the Thomas-Fermi and Molière screening functions.

carbon-carbon potential of Genthon. Also pictured are the Thomas-Fermi and Molière screening factors. While our fits can be somewhat rough, they represent their respective phenomenological potentials considerably better than does the Thomas-Fermi screening factor. Consequently, our cross sections are an improvement over the LNS or WSS (Thomas-Fermi) cross sections.

In Figs. 12 and 13 we show the stopping power for C-C and U-U, respectively. For carbon, as we might expect from Fig. 11, the Molière cross section overestimates the stopping power nearly as much as does the Thomas-Fermi, but because the characteristic energy (Z^2e^2/a) is low for carbon, even the Thomas-Fermi cross section is reasonably accurate. For uranium, both our cross section and the Molière give good results. The Thomas-Fermi gives much too high a stopping power, and does so over a considerable energy range.

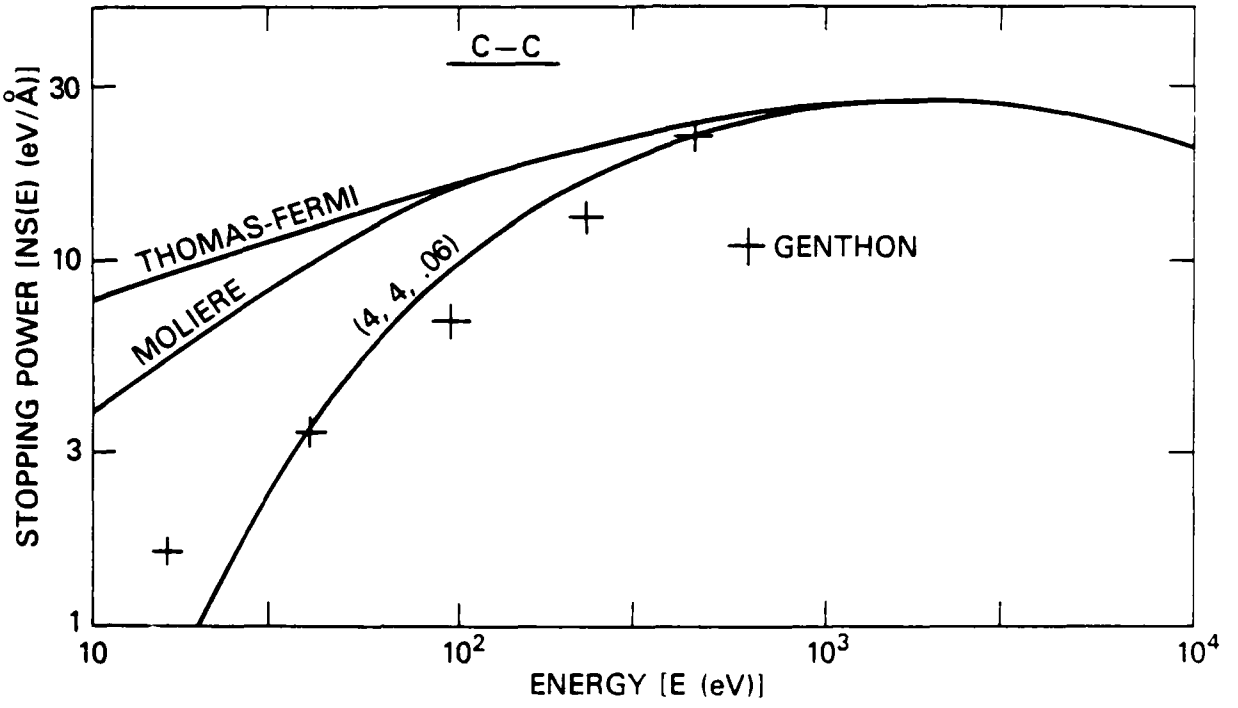

Fig. 12 — Comparison of stopping powers for carbon in carbon based on the Genthon, Molière, Thomas-Fermi, and (4,4, .06) cross sections.

As a final example, we note that the phenomenological interatomic potentials are sometimes of pure Born-Mayer form $V(r) = V' \exp(-\beta' r)$, with the parameters adjusted so that the potential reproduces some crystalline properties of the material.[27] In these cases the potential is clearly not intended for use at high energies; Torrens suggests a restriction to the range for which $V(r) < \frac{1}{3}V'$. The results of using our procedure with a Born-Mayer potential is that we automatically extend its useful range for radiation damage calculations. As an example, in Fig. 14 we show the Gibson #2 potential for copper.[1] Also shown is the potential corresponding to our (2,3, .015) cross section. Our procedure has not only yielded a cross section corresponding to the given potential, but a cross section that has a wider applicability than the original potential could justify.

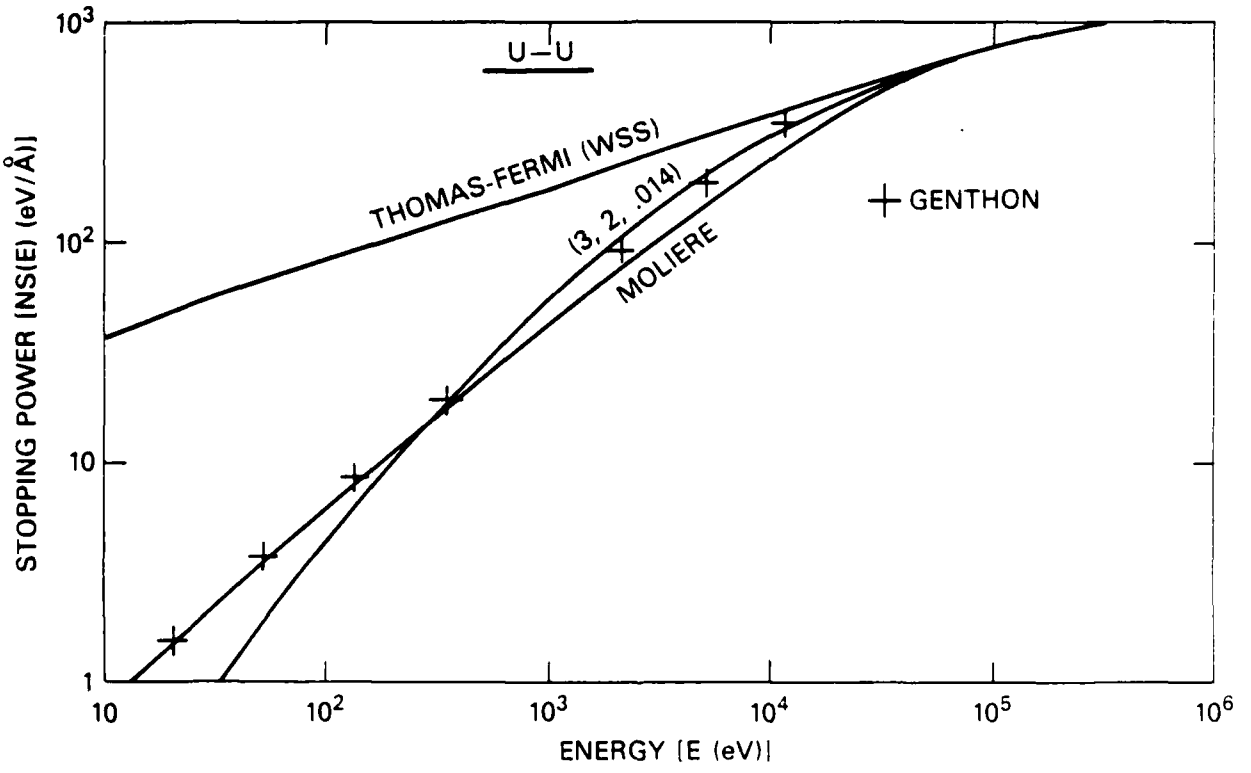

Fig. 13 — Comparison of stopping powers for uranium in uranium based on the Genthon, Molière, Thomas-Fermi, and (3,2, .014) cross sections.

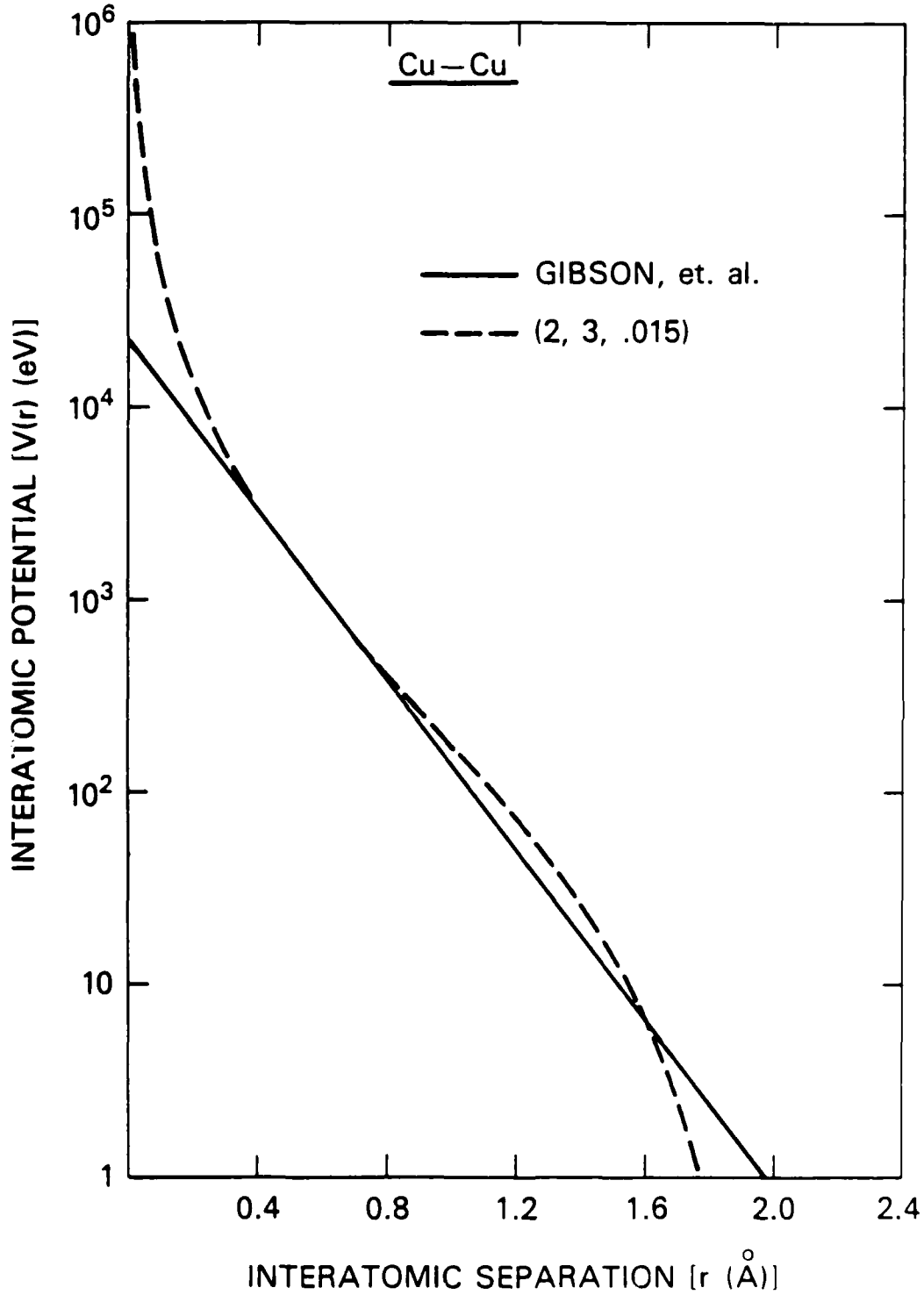

Fig. 14 — Comparison of the potential based on the (2,3, .015) cross section to the copper-copper potential of Gibson, et al.

One question remains. What cross section do we use when we have no phenomenological potential to guide us? In the light of the wide use of the Molière potential for radiation damage problems, and the fact that the Molière fares reasonably well in most of the comparisons we have made in this paper, we suggest our (finite range) version of the Molière cross section with the Firsov screening radius as a universal cross section. Following the procedure discussed earlier, we choose the (3,2, .019) cross section to represent the Molière cross section. In Fig. 15 we compare the reduced stopping power ($NS(E)/(N \pi a^2 E_L)$) for the Molière and (3,2, .019) cross sections. They are in good agreement for all but the lowest values of (reduced) energy transfer. No universal cross section is going to be more than adequate, in general, but in every case we have examined in detail, the (3,2, .019) cross section would be an improvement over the Thomas-Fermi (LNS) form.

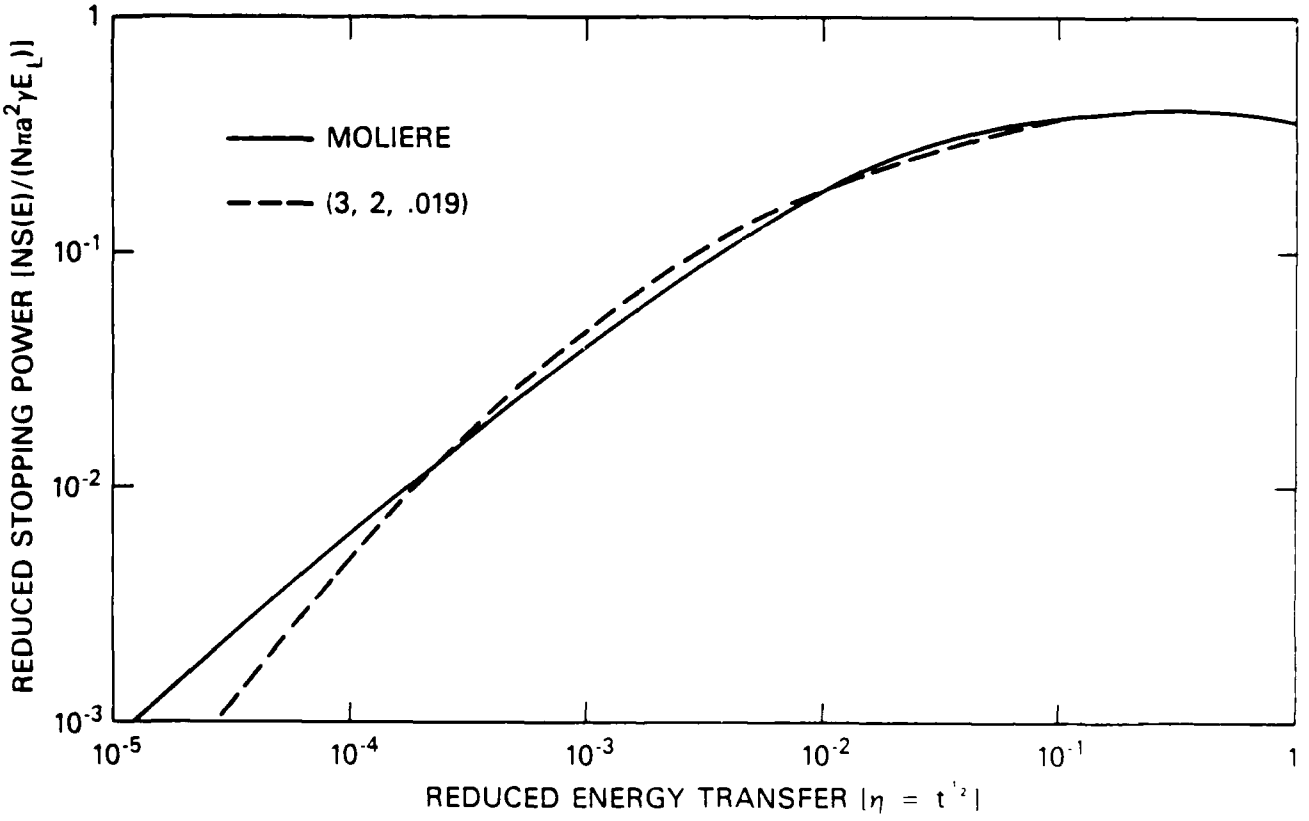

Fig. 15 — Comparison of the reduced stopping power for the Molière cross section with that of the (3,2, .019).

DISCUSSION

We had as our goal in this paper to create a class of cross sections for atomic scattering that were both phenomenologically based and easy to use. We have compared our cross sections to others in two ways; by comparing the corresponding potentials or screening factors, and by comparing the stopping powers derived from each cross section. We have not compared total cross sections because they are infinite for the Thomas-Fermi and Molière forms. Also, we have not compared the square fluctuations in energy loss (Eq. (A4)) because this quantity depends on the higher energy portion of the kernels of the cross sections, and at higher energies the kernels all agree.

We can now ask what differences might result from the use of these new cross sections, relative to using those based strictly on the Thomas-Fermi potential. We have no definite answer, but we can learn something of this matter by examining the curves for stopping power that we showed earlier. In particular, consider Fig. 10 for copper. The calculated range of a copper ion with an initial energy of more than a few keV will be the same whether it is estimated using our new cross sections or the Thomas-Fermi, because the stopping powers for the two cases are the same. Similarly, the (initial) energy deposition curve (energy lost versus depth) for the impinging ion will be the same for both cross sections.

Differences may arise, however, when the motion of the primary knock-on atoms (PKAs) is considered. A typical PKA will have an energy of a few keV, and secondary knock-on atoms will typically have energies of a few hundred electron volts. We see from Fig. 10 that at these energies the Thomas-Fermi stopping power is considerably higher than is the phenomenologically based value. Consequently, the knock-on atoms will have longer ranges than the Thomas-Fermi results would indicate, which may affect the final energy deposition and displacement damage results.

Another difference arises in calculations of energy partitioning. An impinging ion's energy in given up to two mechanisms: transfers of energy to electrons in the bulk material, called inelastic or electronic losses; and transfers of energy to the lattice ions, called elastic losses or damage energy. Some of the elastic losses produce displacements. If the elastic scattering cross section is lowered, then a higher proportion of the initial energy goes into inelastic losses and fewer displacements are produced.[28,29]

ACKNOWLEDGEMENTS

I would like to thank I. Manning for several interesting suggestions and M. Rosen for a thoughtful reading of the manuscript.

APPENDIX A: TOTAL CROSS SECTIONS AND RELATED QUANTITIES

From Eqs. (9, 17-20) we can write

$$N\,\sigma(E) = N\pi a^2\, I(\epsilon) \tag{A1}$$

$$N\,S(E) = N\pi a^2\, \tau\, E_L\, \epsilon^{-1}\, J(\epsilon) \tag{A2}$$

$$N\,\sigma(E) = N\pi a^2\, [\tau\, E_L\, \epsilon^{-1}]^2\, K(\epsilon) \tag{A3}$$

to represent the total cross section, stopping power, and square fluctuation in energy loss, where

$$I(\epsilon) = \int_0^{\epsilon} d\phi\ \ \phi^{-2}\ \ f(\phi) \tag{A4}$$

$$J(\epsilon) = \int_0^{\epsilon} d\phi\ \ f(\phi) \tag{A5}$$

$$I(\epsilon) = \int_0^{\epsilon} d\phi\ \ \phi^{2}\ \ f(\phi)\ \ . \tag{A6}$$

For the function $I(\epsilon)$ we can write

$$I(\epsilon) = \begin{cases} I_<(\epsilon), & \epsilon < \phi^* \\ I_>(\epsilon), & \epsilon > \phi^* , \end{cases} \tag{A7}$$

and similarly for $J(\epsilon)$ and $K(\epsilon)$. Recall that $f(\phi)$ is of the form (23-25) and that the parameters A and B are given by Eqs. (26-27).

For our three families of cross sections and for $\epsilon<\phi^*$, we have the following expressions:

$$(n,m) = (3,2)\ ,\ y = B^{-1}\,\epsilon^{1/2}\ , \tag{A8}$$

$$I_<(\epsilon) = A\,B^{-2}\ (2y+y^2)\ \ (1+y)^{-2}\ , \tag{A9}$$

$$J_<(\epsilon) = A\,B^2\,[12\,\ln(1+y) + (1+y)^{-2}\,(y^4-4y^3-18y^2-12y)]\,, \qquad \text{(A10}$$

$$K_<(\epsilon) = (AB^6/15)\,[\,840\,\ln(1+y) +$$

$$(1+y)^{-2}\,(5y^8-8y^7+14y^6-28y^5+70y^4-280y^3-1260y^2-840y)\,]\,; \qquad \text{(A11}$$

$$(n,m) = (2,3)\,,\ y = B^{-1/3}\,\epsilon^{1/4}\,, \qquad \text{(A12}$$

$$I_<(\epsilon) = \frac{4A}{B^{4/3}}\left[\frac{y^2}{3(1+y^3)} - \frac{1}{18}\ln\frac{(1+y)^2}{1-y+y^2} + \frac{1}{3\sqrt{3}}\tan^{-1}\frac{\sqrt{3}\,y}{2-y}\right], \qquad \text{(A13}$$

$$J_<(\epsilon) = 4AB^{4/3}\left[\frac{-28y-21y^4+3y^7}{12(1+y^3)} + \frac{7}{18}\ln\frac{(1+y)^2}{1-y+y^2} + \frac{7}{3\sqrt{3}}\tan^{-1}\frac{\sqrt{3}\,y}{2-y}\right], \qquad \text{(A14}$$

$$K_<(\epsilon) = \tfrac{1}{9}\,AB^4\,[\,60\,\ln(1+y^3)$$

$$+ (1+y^3)^{-1}\,(-60y^3 - 30y^6 + 10y^9 - 5y^{12} + 3y^{15})\,]\,; \qquad \text{(A15}$$

$$(n,m) = (4,4)\,,\quad y = \epsilon/B\,, \qquad \text{(A16}$$

$$I_<(\epsilon) = 1/3\;A\,B^{-1}\,y^3\,(1+y)^{-3}\,, \qquad \text{(A17}$$

$$J_<(\epsilon) = \tfrac{1}{3}\,AB\,[\,(1+y)^{-3}\,(12y + 30y^2 + 22y^3 + 3y^4) - 12\,\ln(1+y)\,] \qquad \text{(A18}$$

$$K_<(\epsilon) = A\,B^3\,y^2\,(\tfrac{1}{3}\,y^4 - y^3)(1+y)^{-3} + 5\,B^2\,J_<(\epsilon)\,. \qquad \text{(A19}$$

For $\epsilon > \phi$, for all of the families, we have

$$I_>(\epsilon) = I_<(\phi^*) + (4c^2)^{-1} \left[(c-2bd)(2\ \ln y - P_1(y)) - 4bc/y \right.$$

$$\left. -(dc - 2b(d^2-2c)\ P_2(y) \right]_{y=\phi^*}^{y=\epsilon} , \qquad \text{(A20}$$

$$J_>(\epsilon) = J_<(\phi^*) + \tfrac{1}{4} \left[(4b-d)\ P_2(y) + P_1(y) \right]_{y=\phi^*}^{y=\epsilon} , \qquad \text{(A21}$$

$$K_>(\epsilon) = K_<(\phi^*) + \tfrac{1}{4} \left[y^2 + (4b-2d)y + (d^2-c-2bd)\ P_1(y) \right.$$

$$\left. +(2b(d^2-2c) - d(d^2-3c))\ P_2(y) \right]_{y=\phi^*}^{y=\epsilon} , \qquad \text{(A22}$$

where

$$P_1(y) = \ln[c+y(d+y)] \qquad \text{(A23}$$

$$P_2(y) = P_0^{-1}\ \ln[(d+2y-P_0)/(d+2y+P_0)] , \qquad \text{(A24}$$

$$P_0 = (d^2 - 4c)^{1/2} . \qquad \text{(A25}$$

APPENDIX B: INVERSION METHOD

Given the approximations that allowed us to take Eq. (5) into Eq. (16), one can easily[18] obtain the potential corresponding to a given cross section according to the prescription

$$V(r) = \frac{Z_1 Z_2 e^2}{a} \frac{4}{\pi} \int_r^\infty dp\, \phi(p)\, [p^2 - r^2]^{-1/2} \quad . \tag{B1}$$

Just as Eq. (14) is the first in a series of approximations to the scattering angle, Eq. (B1) is the first term in what is known as the impact expansion method of expressing the potential in terms of the reduced scattering angle.[30,31,32]

Let us suppose that we have a potential V(r) that vanishes for r>R, and let us write the impact parameter and R in reduced the notation

$$q = p / a \,, \quad Q = R / a \,. \tag{B2}$$

Then Eqs. (16) and (B1), with the use of the approximation (15), can be written

$$\phi(q) = -\frac{1}{2} q \int_q^Q dx\, [x^2 - q^2]^{-1/2} \frac{d}{dx} x^{-1} C(x) \,. \tag{B3}$$

$$C(x) = \frac{4x}{\pi} \int_x^Q dq\, \phi(q)\, [q^2 - x^2]^{-1/2} \quad . \tag{B4}$$

Within the framework of this inversion method, the relationship between the reduced impact parameter and the reduced energy transfer is

$$q^2 = \int_\phi^\infty ds\ s^{-2}\ g(s) \quad , \quad \phi = [T\, E/(\tau\, E_L^{\,2})] \quad . \tag{B5}$$

The cutoff radius is related to the differential cross section by

$$Q^2 = \int_0^\infty d\phi \;\; \phi^{-2} \;\; g(\phi) \quad . \tag{B6}$$

A change of variable from q to ϕ converts Eq. (B4) to the form

$$C(x) = \frac{4\alpha}{\pi} \int_0^{\phi_x} d\phi \;\; [q^2 - x^2]^{-1/2} \qquad \frac{g(\phi)}{2\, q\, \phi} \tag{B7}$$

where ϕ and q are related by Eq. (B5) and ϕ_x is that value of ϕ that satisfies

$$x^2 = \int_{\phi_x}^\infty d\phi \;\; \phi^{-2} \;\; g(\phi) \quad . \tag{B8}$$

As a practical matter, we choose a set of values of ϕ_x and then use Eqs. (B8) and (B7) to determine the corresponding values of the argument x and the screening factor C(x). In effect, we form a table of C(x) versus x.

As a example of the use of this procedure, we use Eq. (B7) to find the potential corresponding to f_W, the WSS form of the LNS kernel. In Fig. 16 we show the actual Thomas-Fermi[13] screening factor and that obtained by the above procedure using $f_W(\phi)$. The difference at large separations reflects the fact that $f_W(\phi)$ falls off more slowly as ϕ goes to 0 than would the equivalent Thomas-Fermi kernel; one can see this be comparing the WSS and LNS kernels in Fig. 4.

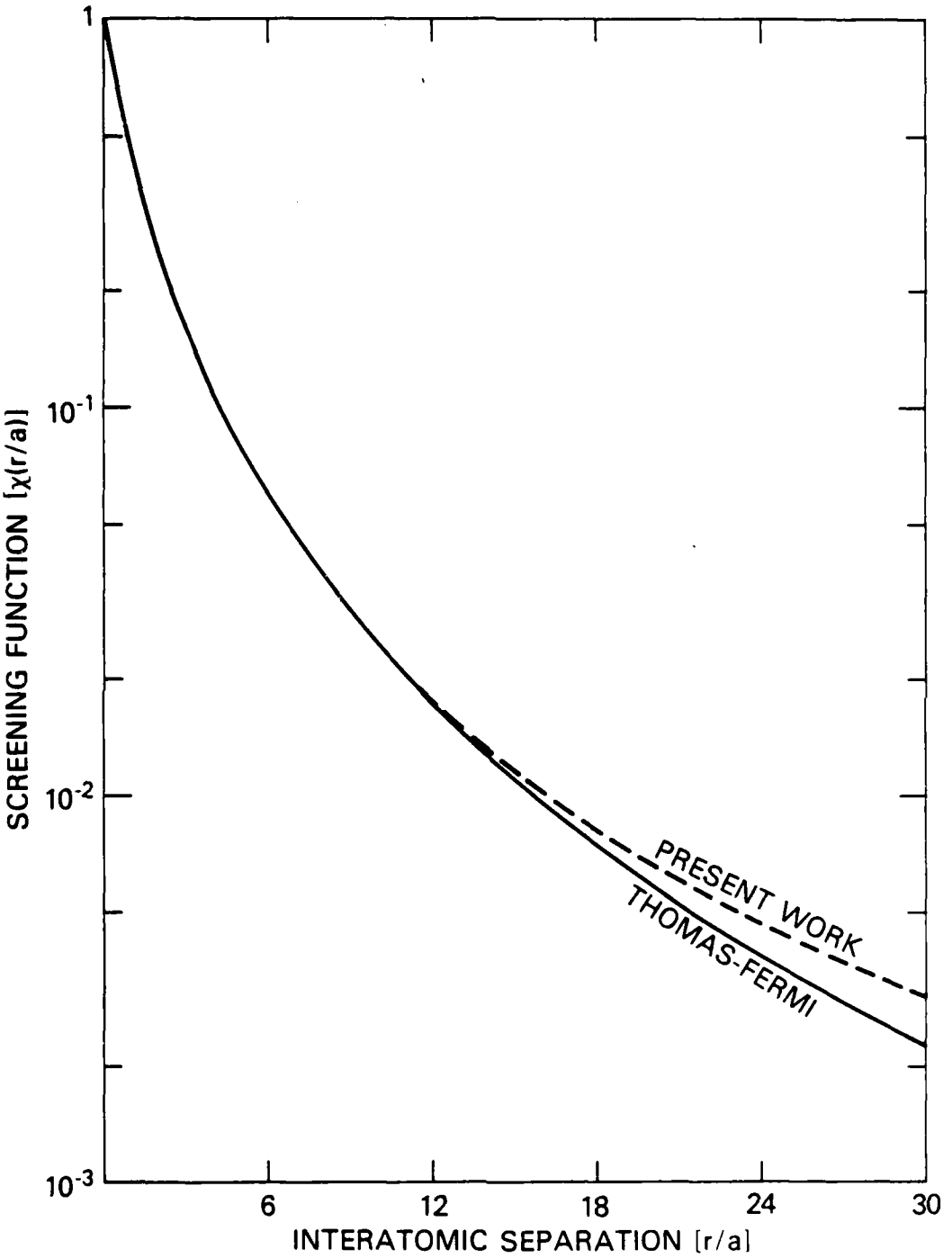

Fig. 16 — Comparison of the actual Thomas-Fermi screening function with the screening function obtained by operating on the WSS cross section with inversion process described in Appendix B.

REFERENCES

1. J.B. Gibson, A.N. Goland, M.Milgram, and G.H. Vineyard, Phys. Rev. 120, 1229 (1960).

2. C. Erginsoy, G.H. Vineyard, and A. Englert, Phys.,Rev. 133, A595 (1964).

3. M.T. Robinson and I.M. Torrens, Phys. Rev. B9, 5008 (1974).

4. J.R. Beeler and D.G. Besco, J. Appl. Phys. 34, 1873 (1963).

5. J. Lindhard, V. Nielsen, and M. Scharff, Kgl. Danske Videnskab. Selskab, Mat.-Fys. Medd. 36, No. 10 (1968).

6. J.Lindhard, M. Scharff, and H.E. Schiott, Kgl. Danske Videnskab. Selskab, Mat-Fys. Medd. 33, No. 14 (1963).

7. J. Lindhard, V. Nielsen, M. Scharff, and P.V. Thomsen, KGl. Danske Videnskab. Selskab, Mat/-Fys. Medd. 33, No. 10 (1963).

8. K.B. Winterbon, P. Sigmund, and J.B. Sanders, Kgl. Danske Videnskab. Selskab, Mat-Fys. Medd. 37. No. 14 (1970).

9. D.K. Brice, Ion Implantation Range and Energy Deposition Distributions (IFI/Plenum, New York, 1975), Vol. I.

10. K. B. Winterbon, Ion Implantation Range and Energy Deposition Distributions (IFI/Plenum, New York, 1975), Vol. II.

11. M.T. Robinson, Phys. Rev. 179, 327 (1966).

12. O.B. Firsov, Zh. Eksp. Teor. Fiz. 33, 696 (1957)[Sov. Phys. JETP 6, 534 (1958)].

13. I.M. Torrens, Interatomic Potentials (Academic Press, New York, 1972), p. 223.

14. G. Molière, Z.Naturforsch. 2a, 133 (1947).

15. Ref. 13, p. 70.

16. I.M. Torrens and M.T. Robinson, in Interatomic Potentials and Simulation of Lattice Defects, ed. by P.C. Gehlen, J.R. Beeler, Jr., and R.I. Jaffee (Plenum, New York, 1972), p. 423.

17. H. Goldstein, Classical Mechanics, 2nd ed. (Addison-Wesley, Cambridge, Mass. 1980), p. 108.

18. G.P. Mueller, NRL Memorandum Report 5624 (1985).

19. Chr. Lehmann and G. Leibfried, Z. Physik 172, 465 (1963).

20. K.B. Winterbon, Atomic Energy of Canada Ltd. Report AECL-3194 (1968).

21. G.P. Mueller, Rad. Effects 21, 253 (1974).

22. I. Manning, private communication.

23. G.P. Mueller, NRL Report 8207 (1978).

24. J.P. Genthon, CEA (France) Rep. No. R-3712 (1969).

25. Ref. 13, p. 69.

26. W.D. Wilson and R.A. Johnson, in Ref. 16, p. 378.

27. Ref. 13, pp. 61-67.

28. G.P. Mueller, Nuc. Inst. Meth. 170, 389 (1980).

29. G.P. Mueller, to be published.

30. F.T. Smith, R.P. Marchi, and K.G. Dedrick, Phys. Rev. 150, 79 (1966).

31. Ref. 13, p. 166.

32. F. Malagutti and F. Verondini, Rad. Effects 19, 121 (1975).